

Genetic, Cellular, and Connectomic Characterization of the Adult Human Brain Regions Commonly Plagued by Glioma

Ayan S. Mandal^{1*}, Rafael Romero-Garcia¹, Michael G. Hart^{1,2}, John Suckling¹

¹Brain Mapping Unit, Department of Psychiatry, University of Cambridge

²Academic Division of Neurosurgery, Department of Clinical Neurosciences, University of Cambridge

* Correspondence to: Ayan Mandal, University of Cambridge, Department of Psychiatry, Herchel Smith Building, Robinson Way, Cambridge, UK CB2 0SZ, Email: asm82@cam.ac.uk

Abstract

A better understanding of the nonrandom localization patterns of gliomas across the brain could lend clues to the origins of these types of tumors. We combined neuroimaging data from 335 adult patients with high- and low-grade glioma to form a replicable tumor frequency map. Using this map, we demonstrate that glioma frequency is elevated in association cortex and correlates with multiple graph-theoretical metrics of high functional connectedness. Brain regions populated with stem-like cells also exhibited a high glioma frequency. Furthermore, gliomas localized to brain regions enriched with the expression of genes associated with chromatin organization and synaptic signaling. Genetic drivers of gliomagenesis were enriched among the transcriptomic correlates of glioma distribution. Finally, a regression model incorporating connectomic, cellular, and genetic factors explained 58% of the variance in glioma frequency. This work synthesizes concepts from network neuroscience and cancer etiology to clarify the mechanisms underlying glioma distribution.

Introduction

Tumor location represents one of the most important prognostic factors for patients suffering from primary brain cancers^{1,2}, yet little is known about the mechanisms that determine the spatial distribution of gliomas across the brain.

The importance of glioma location for diagnosis and treatment has been recognized since Percival Bailey and Harvey Cushing's seminal classification of brain tumors in the early 20th century³. Recent research has demonstrated that tumor location is influenced by the genetic aberrations that guide the development of the tumor^{4,5}. Functional and anatomical differences between regions, such as variations in energy metabolism^{6,7} and brain-wide patterning of canonical cell types^{5,8}, have been hypothesized to play a role in determining glioma distribution. A comprehensive theory for glioma distribution could shed light on the origins of these tumors, and consequently inform treatment targets. Three general hypotheses for the spatial distribution of gliomas include a “connectomic hypothesis”, a “cellular hypothesis”, and a “genetic hypothesis”.

The connectomic hypothesis posits that highly connected brain regions, called hubs, are especially vulnerable to disorder, such as oncogenesis, due to the metabolic costliness of maintaining many connections. The term “connectome” was originally conceived by analogy to the term “genome” and refers to the collection of all connections in the brain⁹. The connectome can be defined at the microscale, in which case the connections represent synaptic links between neurons, or at the macroscale, where the connections can represent anatomical white matter pathways (structural connectome), or correlations in neuronal activity (functional connectome) between brain regions¹⁰. A foundational finding of network neuroscience is that the connectomes of many different species, across multiple scales, all seem to possess a small-world architecture¹¹. In other words, they are composed mostly of short distance connections between neighboring nodes (brain regions or neurons), but with a few long distance connections between distant nodes. The nodes which form many short and long distance connections are crucial for efficient communication across the network. Brain regions with this type of connectivity pattern are called hubs¹². Brain hubs are believed to be “costly” due to the metabolic demand of maintaining many connections¹³, a factor that makes these regions vulnerable to disease^{14–17}. Long distance axonal connections, for instance, are physiologically expensive to maintain since

proteins in the neuron's presynaptic terminal must be produced in the nucleus, and thus must travel the full distance of the axon to reach their target. This factor contributes to the vulnerability of upper motor neurons to degeneration¹⁸. In a similar way, long distance connections important for the construction of large-scale cortical networks also pose a challenge for glial cells (in particular, oligodendrocytes) to support the requisite axonal tracts¹⁹. Furthermore, brain hubs also receive many connections, and therefore are populated with many synapses which impose metabolic demand upon supporting astrocytes²⁰. Metabolic demands on the glial cells of hub regions could contribute to elevated cell turnover, enhancing the likelihood of a cell acquiring an oncogenic mutation during cell division²¹. Metabolic stress could also contribute to oncogenesis via enhanced production of mutagenic reactive oxygen species²². For these reasons, one may expect gliomas to localize to hubs of the brain connectome.

With their shared dedifferentiated and proliferative nature, the commonalities between stem cells and cancer cells have not gone unnoticed among cancer biologists. These commonalities form the basis of the stem cell hypothesis of cancer, which maintains that cancers tend to originate from normal stem and stem-like cells in the body²³⁻²⁵. When applied to adult glioma, this hypothesis points to two clear suspects as possible cells of origin: neural stem cells (NSC's) and oligodendrocyte precursor cells (OPC's)^{24,25}. These cells are not randomly distributed throughout the brain, and therefore their specific localization patterns may help explain the nonrandom distribution of gliomas. The notion that neural stem cells exist and continue to proliferate in the adult human brain is relatively new and historically controversial, but a consensus has arisen that they can be found in at least two locations: the subgranular zone of the dentate gyrus of the hippocampus, and the subventricular zone^{25,26}. Rodent work has demonstrated that OPC's are widely distributed throughout the mammalian brain²⁷. The patterning of OPC's in the adult human brain is unclear, but could be estimated by utilizing brain-wide maps of gene expression patterns^{28,29}.

Finally, it is well-known that oncogenesis is driven by genetic factors. Adult gliomagenesis is ultimately thought to be the result of glial cells acquiring a series of somatic mutations which trigger uncontrollable cell proliferation^{30,31}. Gliomas may be expected to localize to brain regions where the genetic risk factors for the disease are normatively expressed. Furthermore, consequential to the connectomic and cellular hypotheses, we may also expect that brain regions frequented by glioma to be enriched with the expression of genes associated with cell proliferation or metabolically intensive processes required for long distance neuronal signaling.

In this study, we tested the above hypotheses by examining the connectomic, cellular, and genetic correlates of brain regions commonly plagued by glioma. We begin by deriving a replicable tumor frequency map from neuroimaging data of 335 adult patients with high- and low-grade glioma. Using this map, we compare glioma distributions across canonical subnetworks and correlate them with hub measures calculated from averaged functional connectivity data from a large number of healthy individuals. Then, we determine if glioma frequency is elevated among brain regions expected to be enriched with neural stem cells and oligodendrocyte precursor cells. Next, we conduct a transcriptomic analysis to find genes with spatial expression patterns that follow the observed glioma distribution. Finally, we combine all predictive factors of glioma distribution into a single regression model to determine the relationships between predictors of glioma frequency.

Methods

Tumor Frequency Map

Neuroimaging data of patients with low and high grade gliomas were accessed from the Multimodal Brain Tumor Image Segmentation Challenge 2019 (BraTS: <http://braintumorsegmentation.org>)³²⁻³⁴. T1-weighted contrast-enhanced scans from 259 patients with high-grade glioma and 76 patients with low-grade glioma were segmented by board-certified neuroradiologists, denoting voxels that constituted gadolinium enhancing tumor, non-enhancing core, and peritumoral edema³³. Segmentation was informed by multimodal imaging, including T1-weighted, post-contrast T1-weighted, T2-weighted, and T2 Fluid Inversion Attenuated Recovery (T2-FLAIR) scans. Scans were acquired at nineteen different institutions (<https://www.med.upenn.edu/cbica/brats2019/people.html>) with different sequences and protocols. These data were pre-processed through the same pipeline, undergoing linear registration to a common template (SRI24)³⁵, resampling at 1mm³ isotropic resolution, and removing non-brain tissues from the image³⁴.

The minimally pre-processed images were downloaded from the Center for Biomedical Image Computing & Analytics Image Processing Portal (CBICA IPP). Images from each patient were nonlinearly warped to a common template³⁵ using Advanced Normalization Tools software (ANTS)³⁶, with cost function masking of abnormal brain tissue. The registered masks comprising the gadolinium enhancing tumor and non-enhancing core were taken to represent (and hereafter will be referred to as) the tumor mask.

Tumor masks were concatenated across all 335 patients to create a tumor frequency map, where the value at each voxel denotes the percentage of tumors of the sample that overlapped with that voxel (Figure 1A). Smoothing with a 2 mm full width half maximum (FWHM) Gaussian kernel was applied to the map. An unsmoothed version of this map is shown in Supplementary Information (Supplementary Figure 1). To match genetic data for which most of the samples come from one hemisphere²⁸, we mirrored the tumor frequency map to the left hemisphere for the following analyses. Given the large sample size and concordance with other studies^{6,37}, this tumor frequency map was interpreted to represent general glioma spatial distribution.

Tumor Frequency Parcellation

To quantify tumor frequency by common anatomic subdivisions, we applied to the tumor frequency map an in-house 334 region (with 167 left hemisphere regions) parcellation covering 16 subcortical and 318 neocortical areas. This symmetric parcellation was created by applying a back-tracking algorithm that restricts the parcel size to 500 mm² with the Desikan-Killany atlas boundaries as starting points³⁸. Although this parcellation was gray matter based, parcels were extended 4 mm into the white matter to capture tumor frequency in adjacent white matter regions. Tumor frequency for a parcel was calculated by averaging the voxel value (representing percent tumor overlap) of the mirrored tumor frequency map within each LH parcel.

Internal Replicability

The internal replicability of our tumor frequency map was tested by correlating tumor frequency maps derived from randomly assigned, nonoverlapping cohorts of 168 and 167 patients (Groups 1 and 2).

Simultaneously, we tested the generalizability of our results to groups constituted of differing proportions of low grade versus high grade gliomas. The first group (Group 1) had a 50% higher proportion of low grade gliomas (~34%) as the full cohort (~23%), whereas the second group (Group 2) was constituted of a 50% lower proportion of low grade glioma patients (~11%). These tumor frequency maps were constructed with the same processing as that with the full sample (smoothing, mirroring to the left hemisphere, and parcellation). A 95% confidence interval (CI) for the inter-parcel correlation between Group 1 and Group 2 was determined by constructing a distribution of 100 correlation coefficients where different patients were selected for each group.

Statistical Inference of Brain Map Correspondence

Several analyses in this study involved investigating the spatial correspondence between different imaging derived measures. In general, this was accomplished by calculating the measures at each parcel in the common parcellation scheme, then correlating these measures across parcels for hypothesis testing. However, since the spatial resolution (and thus the number of parcels) of any parcellation scheme is essentially arbitrary, the actual degrees of freedom cannot be estimated. This is aggravated by the spatial autocorrelation of measures among neighboring parcels that violates the assumption of independent observations. This issue has been addressed in past studies by use of what is termed a “spin test”^{39–42}. The spin test procedure is described in more detail in the Supplementary Information. In general, it involves comparing the observed inter-parcel correlation between maps of two measures with a distribution of correlations calculated after one of these maps has been spatially permuted in a way that preserves contiguity among brain regions.

Comparison of Glioma Frequency across Canonical Subnetworks

One question of interest was whether gliomas localized to particular brain subnetworks. Seven canonical subnetworks of the brain (https://surfer.nmr.mgh.harvard.edu/fswiki/CorticalParcellation_Yeo2011)⁴³ were mapped onto the tumor frequency map. Violin plots were constructed to compare the distribution of nonzero tumor frequency values between voxels belonging to differing canonical subnetworks.

Functional Connectome

Glioma frequency was compared to regional connectivity (hubness) as quantified by graph theory metrics applied to the functional connectome derived from resting state fMRI data^{44,45} from over 4000 UK BioBank participants (age range 44–78 years; 53% female). The publicly available “dense voxel-wise connectome” of the first UK BioBank cohort (<https://www.fmrib.ox.ac.uk/ukbiobank/>) corresponds with a 4-D image, where each voxel consists of 1200 principal components derived from a group-level PCA⁴⁶. A correlation between voxels across components gives a close, memory efficient approximation to the correlation of BOLD signal calculated across concatenated timepoints from all individual participants⁴⁶. The aforementioned 334 region in-house parcellation, covering both subcortical and cortical regions, was applied to the voxel-wise connectome. PCA loadings for voxels within each parcel were averaged (analogous to a mean timeseries) and correlated between parcels to produce the weights

of a graph (Figure 2C). Diagonal elements and negative correlations were set to zero. The same parcellation was also applied to the lesion overlap map to quantify tumor frequency within each parcel. Tumor frequency for a parcel represented the average percentage of lesion overlap of voxels within that parcel. The common parcellation allowed for comparison between measures of tumor frequency and functional hubness.

Graph Theory Metrics of Hubness

Once the weighted healthy connectome had been constructed, we calculated graph theory metrics of hubness using the Brain Connectivity Toolbox⁴⁷. Hub metrics considered included: nodal strength (sum of all weighted connections for a particular node), betweenness centrality (fraction of all shortest paths in a network that pass through a certain node), clustering coefficient (average weighted connections of triangular subgraphs associated with a node), local efficiency (inverse of the average shortest path length between a node and each other node), eigenvector centrality (the extent to which a given brain region connects other regions with higher centrality), participation coefficient (the strength of connections outside of a node's given module relative to connections within that node's module), and within-module degree z-score (nodal strength of a node within its module, compared to within-module nodal strengths of each other node in the module). To reduce the impact of community affiliation on participation coefficient and within-module degree z-score, community affiliations were designated based off the maximum spatial overlap of each node (i.e. parcel) with one of the seven canonical Yeo subnetworks.

Hub measures were calculated for each of the 334 nodes of the functional connectome. Measures from homotopic nodes were then averaged together, resulting in 167 observations for each subcortical and cortical parcel per hub metric. Many of the hub measures were observed to have a high correlation with nodal strength. Therefore we screened out measures which had a Spearman's correlation of larger than $\rho=0.95$ with nodal strength. This led to the removal of clustering coefficient, local efficiency, and eigenvector centrality from the list of hub metrics. While this threshold is arbitrary, the same result would be reached with thresholds ranging from 0.65 to 0.99 (Supplementary Figure 2). Spearman's correlations were calculated between the remaining hub metrics and tumor frequency and were assessed for significance by comparison to spatially contiguous null models, via the spin test (see Supplementary Information).

Cellular Correlates of Tumor Frequency

To determine whether tumors were more common in regions enriched for neural stem cells (NSC's), we assessed tumor frequency within the two parcels of our 334 region parcellation which most closely align with the subventricular zone and the dentate gyrus: the caudate and the hippocampus. The average tumor frequency between these two parcels was compared to average tumor frequency between 10000 random pairs of parcels.

To determine if tumors were more common in regions enriched for oligodendrocyte precursor cells (OPC's), we compared tumor frequency to an expression map of OPC cell class. This expression map was estimated by assessing transcriptional enrichment of OPC genetic markers using a procedure analogous to²⁹. An OPC gene set was derived from a single cell RNA sequencing study performed on adult postmortem cortical tissue⁴⁸ that determined genes with transcription patterns distinguishing cells by canonical cell types, including excitatory and inhibitory neurons, astrocytes, oligodendrocytes, and OPC's. The set of 132 genes that

distinguished OPC's from other canonical cell classes across the cortex was downloaded from the Supplementary Materials of ⁴⁸. Next, we determined parcels where the OPC gene set was upregulated in the adult brain using the publicly available Allen Human Brain Atlas (AHBA)²⁸. The Allen Human Brain Atlas catalogues postmortem gene expression from six individuals (ages 24 to 57 years old; five males and one female) at a variety of brain locations. Transcription patterns of 20,647 genes was aligned to the 159 LH cortical regions in our parcellation, using methods described in ^{49,50} and code available for download here (https://github.com/RafaelRomeroGarcia/geneExpression_Repository). The resulting 159 x 20,647 regional gene expression matrix was z-scored by parcel. Because the OPC gene set was derived from sequencing performed on cortical brain tissue, we decided to exclude subcortical regions from this part of the analysis.

First, 13 genes in the OPC gene set were not matched to any AHBA probe and were consequently excluded from the analysis. We evaluated the spatial specificity of the remaining 119 OPC genes by comparing their co-expression pattern with 1000 identically-sized sets of randomly chosen genes. OPC genes that did not share a positive coexpression pattern with the overall group of genes were filtered out. Concretely, 24 genes which had, on average, negative correlations with other genes in the set were removed from the OPC gene set. We estimated OPC distribution by calculating the median regional enrichment of the filtered OPC gene set across cortical parcels. OPC distribution across 159 cortical parcels was then correlated with tumor frequency and tested for significance using the spin test.

Aligning Tumor Frequency Map with the Allen Human Brain Atlas

Next, we compared tumor frequency with postmortem gene expression from the Allen Human Brain Atlas (<http://human.brain-map.org/>)²⁸. Pre-processing of the AHBA data followed a similar pipeline to previous work from our group ^{49,50} and is described in more detail in the Supplementary Information. Transcription levels for 20647 genes across 2748 sample locations were related to tumor frequency at each sample location using partial least squares (PLS) regression. Tumor frequency values were aligned with sample locations by warping the non-smoothed, non-mirrored tumor frequency map into MNI space, a standard brain template for which the locations of the AHBA microarray samples are known. Once in MNI space, a 2 mm FWHM smoothing kernel was applied to the map and the map was mirrored to the left hemisphere. Sample locations from the AHBA that were located in the right hemisphere were also mirrored to their homotopic voxel in the left hemisphere. This alignment resulted in a 2748 (samples) by 20647 (genes) expression matrix and in a vector of 2748 elements representing tumor frequency values matched to each sample's MNI coordinates (Figure 4 A,B). Tumor frequency values were square rooted to reduce the skewness of the tumor frequency distribution (Figure 1B). Gene expression values were z-scored for each gene. To test the robustness of the findings, the analyses below were repeated using tumor frequency maps derived from Group 1 and Group 2.

Transcriptomic Correlates of Tumor Frequency

PLS regression was used to relate spatial transcription patterns of 20647 genes with the spatial distribution of glioma. PLS regression involves projecting a predictor (X) and a response (y) matrix into a space where linear combinations of X explain the maximum amount of variance

in y . We chose to focus on the first two components from PLS (PLS 1 and PLS2) as the subsequent components explained indistinguishable variance from one another (Supplementary Figure 3A). Statistical significance of the PLS model was tested via permutation testing, by comparing the percent variance explained in the original model to a distribution of 1000 models where the sample labels mapping X to y were randomly shuffled. Significance of each PLS coefficient was tested via bootstrapping with 1000 iterations, resulting in two Z statistics for each gene, one for the first PLS component and another for the second PLS component. Genes were ranked by their Z statistics and entered into gene ontology analyses in GOrilla (<http://cbl-gorilla.cs.technion.ac.il/>), resulting in a hierarchy of biological terms associated with each PLS component, visualized using Revigo⁵¹. To ensure a data-driven approach, genes with Z statistic values that did not meet the Bonferroni-corrected significance threshold were not excluded from the gene lists.

Relating PLS Components to Glioma-related Genes

We sought to determine whether either of our PLS components were enriched for genes that are dysregulated in glioma. We collected a list of 20 genes from a recent review³⁰ that are known to be either mutated, amplified, or lost in specific subtypes of glioma. Four of these genes (*PDGFRA1*, *RIK*, *RIS*, and *PI3K*) were not matched to any AHBA probe and were accordingly excluded from the analysis.

Similar to the OPC gene list preprocessing, we first confirmed that these genes co-expressed significantly (compared to 10,000 identically sized sets of genes). Next, we filtered out genes with differing co-expression patterns from the group (denoted by negative correlations, on average, with other genes in the set), leading to the exclusion of three genes (*IDH2*, *MYCN*, and *CIC*). The median rank of the final list of 13 genes was determined among the first and second PLS components and assessed for significance by comparison to median ranks expected from chance.

Visualization of PLS Components

We were interested in the locations of the samples which drove each PLS component. First, PLS1 and PLS2 loadings were plotted and colored based of the affiliation of the sample with cortex or subcortex. To determine how PLS1 and PLS2 loadings mapped onto cortex, we assigned samples to parcels via a nearest neighbor mapping. Then, the PLS loading of a parcel was represented as the median PLS loading across samples assigned to that parcel. Two parcels were assigned zero samples from nearest neighbor mapping, and these parcels were assigned the mean loading of the group. More samples were mapped to each subcortical parcel ($N=8$; mean=78.9; SD=52.1) compared to each cortical parcel ($N=159$; mean=13.3; SD=12.5).

Multivariate Model Combining Connectomic, Cellular, and Genetic Contributions to Tumor Frequency

To determine how different measures of biological contributions to glioma risk interrelate, we developed a multiple linear regression model combining each of the factors we found to be associated with tumor frequency. The model included nodal strength, OPC enrichment, PLS1

loadings, and PLS2 loadings. Each of these measures was represented as a 167-dimensional vector, with a value ascribed to each parcel within our parcellation scheme. The dependent variable for the model was the square root of average tumor frequency within each parcel. The square root of tumor frequency was taken to address the skewness of the raw tumor frequency values (Figure 1B). Each of the predictors was z-scored, and zeros were assigned to parcels for which no value could be appropriately calculated (e.g. subcortical parcels for OPC enrichment, and parcels mapped to zero samples for PLS1 and PLS2 loadings).

First, we constructed a model to determine whether there were any two-way interaction effects between the different scales of biological factors. Nodal strength represented “connectomic factors”, OPC enrichment represented “cellular factors”, and PLS1 and PLS2 loadings represented “genetic factors”. This model had the following form:

$$\text{tumor frequency} = b_0 + b_1 * \text{strength} + b_2 * \text{OPC} + b_3 * \text{PLS1} + b_4 * \text{PLS2} + b_5 * \text{strength|OPC} + b_6 * \text{strength|PLS1} + b_7 * \text{strength|PLS2} + b_8 * \text{OPC|PLS1} + b_9 * \text{OPC|PLS2} + \varepsilon$$

This model revealed no significant interactions effects between different biological factors. Therefore, we constructed a second model with no interaction terms, of the form:

$$\text{tumor frequency} = b_0 + b_1 * \text{strength} + b_2 * \text{OPC} + b_3 * \text{PLS1} + b_4 * \text{PLS2} + \varepsilon$$

After determining the percentage of explained variance in tumor frequency from these predictors, we explored the individual contribution of each variable by calculating the square of the partial correlation between that variable and tumor frequency. Significance of the explained variance was assessed by comparison to the distribution of explained variances between the variable and 10000 permuted, spatially contiguous, null models of tumor frequency.

Results

Glioma frequency is replicable across heterogeneous cohorts

A tumor frequency map derived from the full cohort displayed a hemispherically symmetric, but heterogeneous spatial distribution (Figure 1A). Consistent with prior reports, gliomas were rare in the occipital lobe but relatively common in insular cortex (Figure 1B; Supplementary Table 1). Tumor frequency distributions were replicable across independent, randomly assigned subsets of half of the images, Groups 1 and 2, with an inter-parcel correlation of $r=0.83$ (95% CI: $r=0.70-0.93$). Replicability of subsequent analyses were tested with Group 1 and Group 2 tumor frequency maps (see Supplementary Information).

Gliomas most frequently occur in association cortex

Tumor frequency was compared across canonical, large-scale functional networks and primary versus association cortex. Association regions responsible for consolidating information across multiple sensory modalities showed higher tumor prevalence than primary cortex (visual

and somatosensory) which had the lowest tumor frequency, particularly on the visual cortex (Figure 2A and 2B).

Graph theory measures of hubness spatially correlate with glioma frequency

Graph theory measures were calculated from a functional connectome derived from over 4000 UK BioBank participants (Figure 2C) and compared with glioma frequency. Glioma frequency correlated with nodal strength ($\rho = 0.34$; $P_{\text{spin}} = 0.00055$), betweenness centrality ($\rho = 0.51$; $P_{\text{spin}} = 0.0002$), and participation coefficient ($\rho = 0.30$; $P_{\text{spin}} = 0.011$), but not with Z-score modularity ($\rho = 0.062$; $P_{\text{spin}} = 0.21$; Figure 2D).

Glioma frequency is elevated in brain regions expected to be populated with stem-like brain cells

We tested the hypothesis that brain regions enriched with neural stem cells were more likely to coincide with loci of a high frequency of gliomas. Mean tumor frequency was calculated across the parcels denoting the hippocampus and the caudate (Figure 3A), the regions in our parcellation which best approximate the locations of the only known sources of neural stem cells in the adult human brain. Tumor frequency across the hippocampus and caudate were averaged, and compared against a null distribution of 10000 different pairs of randomly selected parcels within our 334-region parcellation scheme. Glioma frequency was observed to be significantly higher in these two regions expected to be populated by neural stem cells compared to the null distribution ($p = 0.0315$; Figure 3B).

Next, we determined that the list of genetic markers for OPC expression co-expressed significantly (Figure 3C), confirming that median expression across this gene list represents a spatially specific phenotype. OPC expression correlated significantly with glioma frequency (Figure 3D; $\rho = 0.45$; $P_{\text{spin}} = 0.0001$).

Transcriptomic correlates of glioma frequency

We used PLS regression to relate spatial transcription patterns across 20647 genes with tumor frequency at 2768 locations where gene expression was assessed in postmortem adult human brain tissue (Figure 4A,B). The first two components of the PLS (PLS1 and PLS2) explained 19% and 18% of the tumor frequency variance, respectively (Supplementary Figure 3A), more than expected by chance (Permutation test; $p < 0.001$; Supplementary Figure 3B). Bootstrapping was performed on PLS weights for each gene, resulting in Z statistics for each gene corresponding to PLS1 and PLS2 ranking (Supplementary Figure 3C). The robustness of the PLS gene ranks was assessed by comparing to gene ranks generated from PLS regressions predicting tumor frequency from Group 1 and Group 2.

Gene lists, ranked by their Z statistic values within PLS1 and PLS2, were entered into gene ontology in GOrilla (<http://cbl-gorilla.cs.technion.ac.il/>). Genes corresponding to PLS1 were related to biological processes such as chromatin organization, endosomal transport, and G0 to G1 transition. Genes corresponding to PLS2 were related to a broad set of metabolic processes along with many components of synaptic transmission (Figure 4C). PLS1 was also found to be significantly enriched for genetic drivers of gliomagenesis ($p = 0.026$; Figure 4D). PLS2 was not significantly enriched for this set of genes ($p = 0.75$).

PLS1 was more highly loaded onto the subcortex relative to the cortex (Figure 4E. PLS loadings for each AHBA sample were mapped to their nearest brain parcel for visualization on the cortical surface (Figure 4F).

Connectomic, cellular, and genetic contributions to glioma frequency are independent

Finally, we sought to reveal the interrelations between the connectomic, cellular, and genetic contributions to glioma distribution uncovered in the study. A multivariate model was constructed, with factors for nodal strength, OPC enrichment, NSC enrichment, PLS1 loadings, and PLS2 loadings. First, we tested a model to determine if there were interaction effects between connectomic (nodal strength), cellular (OPC enrichment and NSC enrichment), and genetic (PLS1 and PLS2 loadings) factors, but none were significant and they were thus omitted from the model. The model explained 58% of the variance in glioma frequency ($F(4,162) = 59.3$; $p = 9.37 \times 10^{-31}$; Adjusted $R^2 = 0.584$). All individual factors predicted a significant amount of tumor frequency variance (Table 1). Because of the unequal mapping of AHBA samples to cortical versus subcortical parcels, the PLS2 component, which is more highly represented across cortex, explains much more of the variance in tumor frequency once projected onto parcels. It is also worth noting that the amount of variance explained by PLS regression is inflated by construction, due to the large number of input variables and the objective of the technique to maximize covariance⁵².

Discussion

In this study, we examined the network, cellular, and transcriptomic correlates of brain regions commonly frequented by glioma to test specific hypotheses regarding gliomagenesis. We found that gliomas were more common in association cortex and connector hub regions. Elevated glioma frequency was observed in brain regions expected to be populated by neural stem cells and oligodendrocyte precursor cells. Finally, we determined that gliomas localized to brain regions enriched with normative expression of genes related to metabolic activity, cell division, and gliomagenesis. This work supports the predictions of network neuroscience and cancer theory as well as links concepts from these two frameworks to characterize the spatial distribution of adult gliomas.

Neurologic disease localizing to hubs

An extensive body of work has demonstrated the utility of network models in predicting the spread of disease^{53–55} as well as the vulnerability of particular brain regions to disease^{14,15,17}. In this work, we use network models for the latter purpose and demonstrate for the first time that gliomas localize to hub regions of the brain, similar to other neuropsychiatric illnesses. In particular, gliomas appear to localize to brain regions expected to play the role of connector hubs, nodes that link diverse cognitive subsystems with one another, as opposed to provincial hubs which integrate communication within their own subsystems¹². This suggests that the brain regions which facilitate long distance connections across cortex are especially vulnerable to oncogenesis, consistent with our hypothesis that the high metabolic cost of such connections influences glioma risk¹³.

In addition to the high metabolic costs of hubs, these results can also be interpreted to reflect a higher likelihood for tumors to infiltrate hub regions. Gliomas are known to migrate throughout the brain via blood vessels and white matter tracts, which contributes to the poor prognosis of glioblastoma multiforme. Here, we consider only the location of the tumor during the pre-operative scan. This location could reflect either where the tumor originated, or where it spread during the progression of the disease. Due to their high centrality, hubs are, by definition, likely to be encountered during random walks within a network. It is important to note that the connections within the network defined in this study are functional links, representing coordinated neuronal activity, not physical white matter tracts which tumors are known to infiltrate⁵⁶. However, recent work on activity-dependent glioma migration⁵⁷ suggests that tumors could preferentially invade functional hubs as well. An important question for future research will be whether gliomas originate in or spread to hub regions of the brain.

Our interpretation of the graph theory findings are limited by the uncertain nature of functional connectivity⁵⁸ and the methodological difficulty of identifying noncontroversial hubs⁵⁹. However, the finding that gliomas localize to association cortex is both consistent with our interpretation of the graph theory results and less dependent on methodological approach. The finding provides support for the “tethering hypothesis”, or the notion that association cortex lacks developmental stability compared to the more evolutionarily conserved primary cortex, introducing vulnerability for neuropsychiatric disorder^{13,60}. Past work has supported the tethering hypothesis within the context of psychiatric diseases such as autism and schizophrenia^{61,62}. The application of the idea to glioma suggests that the extensive scaling of association cortex during hominid evolution, an event purportedly responsible for human-unique cognition, may also have introduced risk for brain cancer. This idea is consistent with the observation that genes likely involved in cortical scaling (e.g. neurodevelopmental genes guiding proliferation of neural and glial cells) are affected in glioma⁶³.

Cells of origin for glioma

Early work on gliomagenesis hypothesized that mature glial cells were the cells of origin for adult glioma, given the prevailing view at the time that neural stem cells were absent in the adult human brain²⁵. However, it is unlikely that the cell of origin for glioma will be nondividing since the cell must accumulate a number of mutations before it becomes cancerous, improbable to occur within the lifespan of a single glial cell²⁵. Following recent evidence that neural stem cells do reside in the subventricular zone and dentate gyrus of the hippocampus of adults, the field is reaching a consensus that stem-like cells, such as neural stem cells and oligodendrocyte precursor cells, can represent cells of origin for glioma. Recent work from Lee and colleagues provided strong evidence that some IDH-wildtype glioblastomas originate from stem cells in the subventricular zone⁶⁴. They isolated samples from glioblastoma patients within the tumor and the tumor-free subventricular zone and demonstrated that in 56.3% of patients, normal subventricular zone tissue carried low-level driver mutations present at a higher level in the tumor. Our findings complement this research by establishing that gliomas in general are more highly concentrated in regions enriched with neural stem cells.

Oligodendrocyte precursor cells have also been hypothesized to represent cells of origin for glioma. Evidence for this hypothesis comes from studies demonstrating that some gliomas express OPC genetic markers^{65,66}, and that OPC's can be experimentally manipulated into becoming cancer stem cells^{67,68}. OPC's comprise the majority of dividing cells in the adult brain

and are distributed broadly throughout the subventricular zone, white matter, and gray matter^{24,27}. We attempted to estimate this distribution by quantifying normative expression levels of OPC genetic markers across the human brain and demonstrated that this measure correlates with glioma frequency. While this result aligns nicely with prior work, it is worth noting that our estimate of OPC distribution is quite indirect, relying on combining data from two independent transcriptomic studies of post-mortem human brains^{28,48}. While this approach has been validated for determining the brain-wide distribution of other canonical cell types²⁹, our result should be confirmed once a more reliable estimate of OPC patterning across the human brain becomes available.

Genetic determinants of glioma vulnerability

Important work on the genetic basis of cancer over the past decades has determined that normal cells can become cancer cells through a series of somatic mutations which disable tumor suppressors and activate drivers of cell proliferation⁶⁹. To determine the genetic alterations involved in oncogenesis, much of the research has focused on identifying molecular genetic differences between tumor cells and matched healthy tissue^{70,71}. Here, we took an alternative approach and investigated transcriptomic differences between healthy regions where tumors tend to occur versus healthy regions where tumors are uncommon. As expected, this approach recapitulates prior research into glioma genetics, in that genes which drive gliomagenesis appear to be upregulated among the healthy transcriptomic correlates of glioma distribution. Gene ontology revealed that the genes driving PLS1 (the component responsible for most of the covariance between transcription and glioma distribution) were most strongly associated with chromatin organization, a process perturbed by IDH mutations and critically involved in the pathogenesis of glioma^{31,72}. In addition, our approach also reveals novel findings, such as the carcinogenic vulnerability of healthy brain regions enriched with genes coordinating synaptic signaling and metabolic activity. These findings complement our connectomic results, providing more evidence for the idea that metabolically demanding brain regions crucial for brain-wide communication are susceptible to oncogenesis.

The goal of this study was to examine brain regions generally implicated in adult glioma. However, adult glioma is a heterogeneous phenomenon, comprising of tumors of differing genetic etiologies and morphologies. It is known that different types of glioma tend to localize to different brain regions^{4-6,8}. Therefore, the exact composition of patients (e.g. proportion of high grade to low grade glioma patients) within our sample could influence the results. To address this concern, we replicated our results with subgroups of varying proportions of high-grade to low-grade glioma patients and demonstrated that our results are robust to changes to the composition of the sample. However, we did not have access to the molecular genetic characterization of the tumors in our sample, limiting our ability to determine the effect of tumor genotype on the results. Examining glioma subtypes separately could illuminate the network, cellular, and transcriptomic correlates which distinguish localization patterns of different types of glioma. Such work could be useful for developing scientifically informed priors for tumor diagnosis before biopsy, so this question is of both scientific and clinical interest.

Conclusion

Gaining a better understanding of the mechanisms driving glioma localization patterns could prove useful for uncovering the etiology of the disease and consequently inform treatment targets. We demonstrate that glioma distribution can in part be explained by functional hubness, distribution of stem-like cells, and transcription patterns of genetic determinants of glioma. These results add to previous literature reporting the vulnerability of hub regions to neurological disease^{13,14}, as well as provide support for cancer stem cell theories of glioma^{23,25,26}. Our approach could be used to reveal the mechanisms responsible for the spatial distributions of other types of cancer, thus offering a fresh angle to the study of oncogenesis.

Acknowledgements

We thank the Brain Tumor Segmentation Challenge (BraTS) for access to the MRI scans and lesion masks used in the study, as well as the patients who participated in that project. This research also relied on imaging data from UK BioBank and genetic data from the Allen Brain Institute. A.S.M. was funded by a Gates Cambridge Scholarship. R.R.G. was funded by a Guarantors of Brain fellowship. Data were stored and processed on the High Performance Hub for Clinical Informatics (HPHI) platform, funded by a Medical Research Council (MRC) infrastructure award (MR/M009041/1).

Author Contributions

A.S.M., R.R.G., and M.G.H conceived of the research idea. A.S.M. performed the analyses, with R.R.G., M.G.H, and J.S. supervising the work. A.S.M. drafted the article. All authors discussed the results and commented on the manuscript.

Competing Interests

None.

Ethics Statement

The research described in this manuscript used anonymized data made publicly available via the International Brain Tumor Segmentation (BraTS) challenge. All other data considered here had similarly been anonymized before being made publicly accessible.

References

1. Jeremic, B. *et al.* Influence of extent of surgery and tumor location on treatment outcome of patients with glioblastoma multiforme treated with combined modality approach. *J. Neurooncol.* (1994). doi:10.1007/BF01052902
2. Sagberg, L. M. *et al.* Brain atlas for assessing the impact of tumor location on perioperative quality of life in patients with high-grade glioma: A prospective population-based cohort study. *NeuroImage Clin.* (2019). doi:10.1016/j.nicl.2019.101658
3. Bailey, P. & Cushing, H. A Classification of the Tumors of the Glioma Group on a Histogenetic Basis with a Correlated Study of Prognosis. *Arch. Neurol. Psychiatry* (1926). doi:10.1001/jama.1926.02680040056039
4. Tejada Neyra, M. A. *et al.* Voxel-wise radiogenomic mapping of tumor location with key molecular alterations in patients with glioma. *Neuro. Oncol.* (2018). doi:10.1093/neuonc/noy134
5. Zlatescu, M. C. *et al.* Tumor location and growth pattern correlate with genetic signature in oligodendroglial neoplasms. *Cancer Res.* (2001).
6. Duffau, H. & Capelle, L. Preferential brain locations of low-grade gliomas. *Cancer* (2004). doi:10.1002/cncr.20297
7. Duffau, H. *Diffuse low-grade gliomas in adults. Diffuse Low-Grade Gliomas in Adults* (2017). doi:10.1007/978-3-319-55466-2
8. Mueller, W. *et al.* Genetic signature of oligoastrocytomas correlates with tumor location and denotes distinct molecular subsets. *Am. J. Pathol.* (2002). doi:10.1016/S0002-9440(10)64183-1
9. Seung, S. *Connectome: how the brain's wiring makes us who we are.* (Houghton Mifflin Harcourt, 2012).
10. Bullmore, E. & Sporns, O. Complex brain networks: Graph theoretical analysis of structural and functional systems. *Nature Reviews Neuroscience* (2009). doi:10.1038/nrn2575
11. Bassett, D. S. & Bullmore, E. Small-world brain networks. *Neuroscientist* (2006). doi:10.1177/1073858406293182
12. van den Heuvel, M. P. & Sporns, O. Network hubs in the human brain. *Trends in Cognitive Sciences* (2013). doi:10.1016/j.tics.2013.09.012
13. Bullmore, E. & Sporns, O. The economy of brain network organization. *Nature Reviews Neuroscience* (2012). doi:10.1038/nrn3214
14. Crossley, N. A. *et al.* The hubs of the human connectome are generally implicated in the anatomy of brain disorders. *Brain* (2014). doi:10.1093/brain/awu132
15. Warren, D. E. *et al.* Network measures predict neuropsychological outcome after brain injury. *Proc. Natl. Acad. Sci. U. S. A.* (2014). doi:10.1073/pnas.1322173111
16. Aerts, H., Fias, W., Caeyenberghs, K. & Marinazzo, D. Brain networks under attack: Robustness properties and the impact of lesions. *Brain* (2016). doi:10.1093/brain/aww194
17. Seeley, W. W., Crawford, R. K., Zhou, J., Miller, B. L. & Greicius, M. D. Neurodegenerative Diseases Target Large-Scale Human Brain Networks. *Neuron* (2009). doi:10.1016/j.neuron.2009.03.024
18. Nijssen, J., Comley, L. H. & Hedlund, E. Motor neuron vulnerability and resistance in amyotrophic lateral sclerosis. *Acta Neuropathologica* (2017). doi:10.1007/s00401-017-1708-8

19. Buzsáki, G., Geisler, C., Henze, D. A. & Wang, X. J. Interneuron Diversity series: Circuit complexity and axon wiring economy of cortical interneurons. *Trends in Neurosciences* (2004). doi:10.1016/j.tins.2004.02.007
20. Magistretti, P. J. & Allaman, I. A Cellular Perspective on Brain Energy Metabolism and Functional Imaging. *Neuron* (2015). doi:10.1016/j.neuron.2015.03.035
21. Wodarz, D. Effect of stem cell turnover rates on protection against cancer and aging. *J. Theor. Biol.* (2007). doi:10.1016/j.jtbi.2006.10.013
22. Rinaldi, M. *et al.* ROS and brain gliomas: An overview of potential and innovative therapeutic strategies. *International Journal of Molecular Sciences* (2016). doi:10.3390/ijms17060984
23. Visvader, J. E. Cells of origin in cancer. *Nature* (2011). doi:10.1038/nature09781
24. Jiang, Y. & Uhrbom, L. On the origin of glioma. *Ups. J. Med. Sci.* (2012). doi:10.3109/03009734.2012.658976
25. Sanai, N., Alvarez-Buylla, A. & Berger, M. S. Neural Stem Cells and the Origin of Gliomas. *N. Engl. J. Med.* (2005). doi:10.1056/nejmra043666
26. Ma, D. K., Bonaguidi, M. A., Ming, G. L. & Song, H. Adult neural stem cells in the mammalian central nervous system. *Cell Research* (2009). doi:10.1038/cr.2009.56
27. Hughes, E. G., Kang, S. H., Fukaya, M. & Bergles, D. E. Oligodendrocyte progenitors balance growth with self-repulsion to achieve homeostasis in the adult brain. *Nat. Neurosci.* (2013). doi:10.1038/nn.3390
28. Hawrylycz, M. J. *et al.* An anatomically comprehensive atlas of the adult human brain transcriptome. *Nature* (2012). doi:10.1038/nature11405
29. Seidlitz, J. *et al.* Transcriptomic and Cellular Decoding of Regional Brain Vulnerability to Neurodevelopmental Disorders. *bioRxiv* (2019). doi:10.1101/573279
30. Molinaro, A. M., Taylor, J. W., Wiencke, J. K. & Wrensch, M. R. Genetic and molecular epidemiology of adult diffuse glioma. *Nat. Rev. Neurol.* **15**, (2019).
31. Reifenberger, G., Wirsching, H. G., Knobbe-Thomsen, C. B. & Weller, M. Advances in the molecular genetics of gliomas-implications for classification and therapy. *Nature Reviews Clinical Oncology* (2017). doi:10.1038/nrclinonc.2016.204
32. Menze, B. H. *et al.* The Multimodal Brain Tumor Image Segmentation Benchmark (BRATS). *IEEE Trans. Med. Imaging* (2015). doi:10.1109/TMI.2014.2377694
33. Bakas, S. *et al.* Advancing The Cancer Genome Atlas glioma MRI collections with expert segmentation labels and radiomic features. *Sci. Data* (2017). doi:10.1038/sdata.2017.117
34. Bakas, S. *et al.* Identifying the Best Machine Learning Algorithms for Brain Tumor Segmentation, Progression Assessment, and Overall Survival Prediction in the BRATS Challenge. *arXiv* (2018).
35. Rohlfing, T., Zahr, N. M., Sullivan, E. V. & Pfefferbaum, A. The SRI24 multichannel atlas of normal adult human brain structure. *Hum. Brain Mapp.* (2010). doi:10.1002/hbm.20906
36. Avants, B. B., Tustison, N. & Song, G. Advanced Normalization Tools (ANTs). *Insight J.* 1–35 (2009). doi:http://hdl.handle.net/10380/3113
37. Larjavaara, S. *et al.* Incidence of gliomas by anatomic location. *Neuro. Oncol.* (2007). doi:10.1215/15228517-2007-016
38. Romero-Garcia, R., Atienza, M., Clemmensen, L. H. & Cantero, J. L. Effects of network resolution on topological properties of human neocortex. *Neuroimage* (2012). doi:10.1016/j.neuroimage.2011.10.086

39. Alexander-Bloch, A., Raznahan, A., Bullmore, E. & Giedd, J. The convergence of maturational change and structural covariance in human cortical networks. *J. Neurosci.* (2013). doi:10.1523/JNEUROSCI.3554-12.2013
40. Vandekar, S. N. *et al.* Topologically dissociable patterns of development of the human cerebral cortex. *J. Neurosci.* (2015). doi:10.1523/JNEUROSCI.3628-14.2015
41. Alexander-Bloch, A. F. *et al.* On testing for spatial correspondence between maps of human brain structure and function. *Neuroimage* (2018). doi:10.1016/j.neuroimage.2018.05.070
42. Váša, F. *et al.* Adolescent tuning of association cortex in human structural brain networks. *Cereb. Cortex* (2018). doi:10.1093/cercor/bhx249
43. Thomas Yeo, B. T. *et al.* The organization of the human cerebral cortex estimated by intrinsic functional connectivity. *J. Neurophysiol.* (2011). doi:10.1152/jn.00338.2011
44. Miller, K. L. *et al.* Multimodal population brain imaging in the UK Biobank prospective epidemiological study. *Nat. Neurosci.* (2016). doi:10.1038/nn.4393
45. Alfaro-Almagro, F. *et al.* Image processing and Quality Control for the first 10,000 brain imaging datasets from UK Biobank. *Neuroimage* (2018). doi:10.1016/j.neuroimage.2017.10.034
46. Smith, S. M., Hyvärinen, A., Varoquaux, G., Miller, K. L. & Beckmann, C. F. Group-PCA for very large fMRI datasets. *Neuroimage* (2014). doi:10.1016/j.neuroimage.2014.07.051
47. Rubinov, M. & Sporns, O. Complex network measures of brain connectivity: Uses and interpretations. *Neuroimage* **52**, 1059–1069 (2010).
48. Lake, B. B. *et al.* Integrative single-cell analysis of transcriptional and epigenetic states in the human adult brain. *Nat. Biotechnol.* (2018). doi:10.1038/nbt.4038
49. Romero-Garcia, R. *et al.* Structural covariance networks are coupled to expression of genes enriched in supragranular layers of the human cortex. *Neuroimage* (2018). doi:10.1016/j.neuroimage.2017.12.060
50. Romero-Garcia, R. *et al.* Schizotypy-related magnetization of cortex in healthy adolescence is co-located with expression of schizophrenia-related genes. *Biol. Psychiatry* (2019). doi:10.1016/j.biopsych.2019.12.005
51. Supek, F., Bošnjak, M., Škunca, N. & Šmuc, T. Revigo summarizes and visualizes long lists of gene ontology terms. *PLoS One* (2011). doi:10.1371/journal.pone.0021800
52. Mufford, M. S. *et al.* Neuroimaging genomics in psychiatry-a translational approach. *Genome Medicine* (2017). doi:10.1186/s13073-017-0496-z
53. Henderson, M. X. *et al.* Spread of α -synuclein pathology through the brain connectome is modulated by selective vulnerability and predicted by network analysis. *Nat. Neurosci.* (2019). doi:10.1038/s41593-019-0457-5
54. Zhou, J., Gennatas, E. D., Kramer, J. H., Miller, B. L. & Seeley, W. W. Predicting Regional Neurodegeneration from the Healthy Brain Functional Connectome. *Neuron* (2012). doi:10.1016/j.neuron.2012.03.004
55. Brown, J. A. *et al.* Patient-Tailored, Connectivity-Based Forecasts of Spreading Brain Atrophy. *Neuron* (2019). doi:10.1016/j.neuron.2019.08.037
56. Pedersen, P. -H *et al.* Migratory patterns of lac-z transfected human glioma cells in the rat brain. *Int. J. Cancer* (1995). doi:10.1002/ijc.2910620620
57. Venkatesh, H. S. *et al.* Electrical and synaptic integration of glioma into neural circuits. *Nature* (2019). doi:10.1038/s41586-019-1563-y

58. Buckner, R. L., Krienen, F. M. & Yeo, B. T. T. Opportunities and limitations of intrinsic functional connectivity MRI. *Nature Neuroscience* (2013). doi:10.1038/nn.3423
59. Power, J. D., Schlaggar, B. L., Lessov-Schlaggar, C. N. & Petersen, S. E. Evidence for hubs in human functional brain networks. *Neuron* (2013). doi:10.1016/j.neuron.2013.07.035
60. Buckner, R. L. & Krienen, F. M. The evolution of distributed association networks in the human brain. *Trends in Cognitive Sciences* (2013). doi:10.1016/j.tics.2013.09.017
61. van den Heuvel, M. P. *et al.* Evolutionary modifications in human brain connectivity associated with schizophrenia. *Brain* (2019). doi:10.1093/brain/awz330
62. Wei, Y. *et al.* Genetic mapping and evolutionary analysis of human-expanded cognitive networks. *Nat. Commun.* (2019). doi:10.1038/s41467-019-12764-8
63. Puchalski, R. B. *et al.* An anatomic transcriptional atlas of human glioblastoma. *Science* (80-.). (2018). doi:10.1126/science.aaf2666
64. Lee, J. H. *et al.* Human glioblastoma arises from subventricular zone cells with low-level driver mutations. *Nature* (2018). doi:10.1038/s41586-018-0389-3
65. Shoshan, Y. *et al.* Expression of oligodendrocyte progenitor cell antigens by gliomas: Implications for the histogenesis of brain tumors. *Proc. Natl. Acad. Sci. U. S. A.* (1999). doi:10.1073/pnas.96.18.10361
66. Verhaak, R. G. W. *et al.* Integrated Genomic Analysis Identifies Clinically Relevant Subtypes of Glioblastoma Characterized by Abnormalities in PDGFRA, IDH1, EGFR, and NF1. *Cancer Cell* (2010). doi:10.1016/j.ccr.2009.12.020
67. Kondo, T. & Raff, M. Oligodendrocyte precursor cells reprogrammed to become multipotential CNS stem cells. *Science* (80-.). (2000). doi:10.1126/science.289.5485.1754
68. Liu, C. *et al.* Mosaic analysis with double markers reveals tumor cell of origin in glioma. *Cell* (2011). doi:10.1016/j.cell.2011.06.014
69. Mukherjee, S. The Emperor of All Maladies: A Biography of Cancer. *J. Postgrad. Med. Educ. Res.* (2012). doi:10.5005/jp-journals-10028-1025
70. Tang, J., He, D., Yang, P., He, J. & Zhang, Y. Genome-wide expression profiling of glioblastoma using a large combined cohort. *Sci. Rep.* (2018). doi:10.1038/s41598-018-33323-z
71. McLendon, R. *et al.* Comprehensive genomic characterization defines human glioblastoma genes and core pathways. *Nature* (2008). doi:10.1038/nature07385
72. Suzuki, H. *et al.* Mutational landscape and clonal architecture in grade II and III gliomas. *Nat. Genet.* (2015). doi:10.1038/ng.3273

Predictor	Beta Value	Standard Error	T Statistic	Percent Explained Variance	Spin Test Corrected P Value
Intercept	2.01	0.0375	53.7	NA	NA
Nodal strength	0.151	0.0407	3.72	7.86%	0.0011
OPC enrichment	0.155	0.0425	3.64	7.58%	0.0036
PLS1 Loadings	0.158	0.0445	3.54	7.17%	0.0056
PLS2 Loadings	0.360	0.0432	8.32	29.9%	0

Table 1. Results of multiple linear regression model predicting tumor frequency.

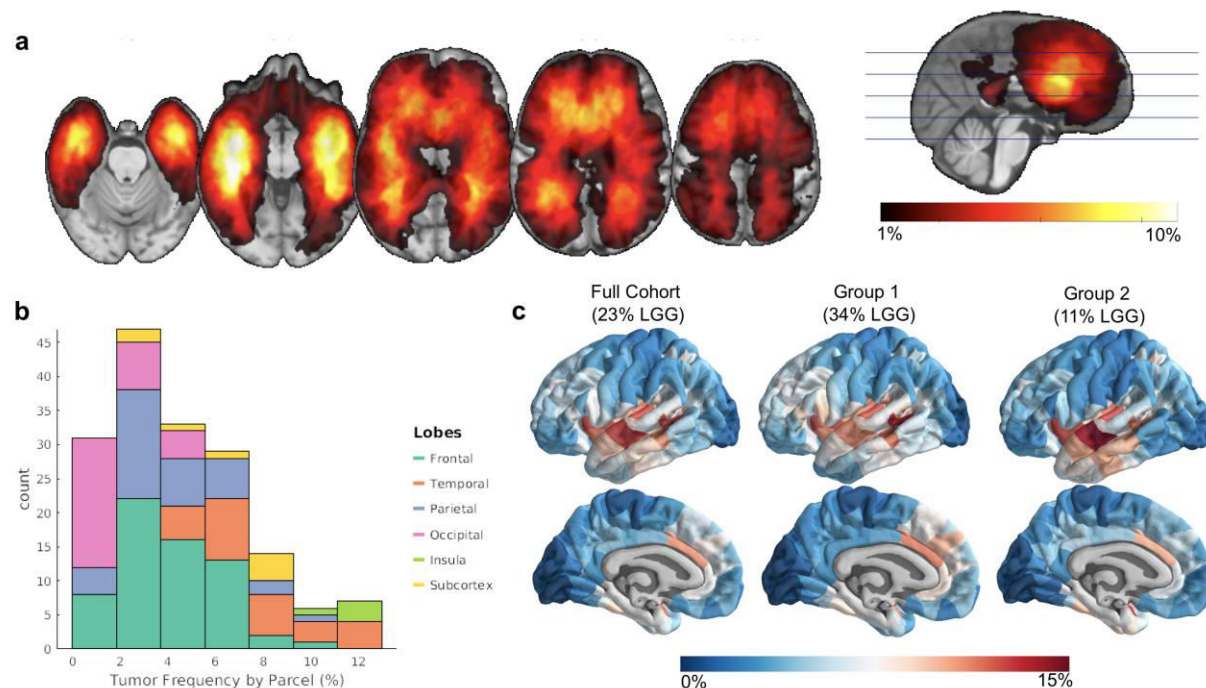


Figure 1. Non-random spatial distribution of gliomas. A. Tumor frequency map derived from lesion masks from 335 patients with high- and low- grade glioma. B. Glioma frequency by common anatomic subdivisions. C. Glioma frequency represented at a parcel-level. Internal replicability of glioma frequency tested by constructing two independent maps from even splits of the cohort, where the first comprised of ~34% low grade gliomas and the other of ~11% LGG's.

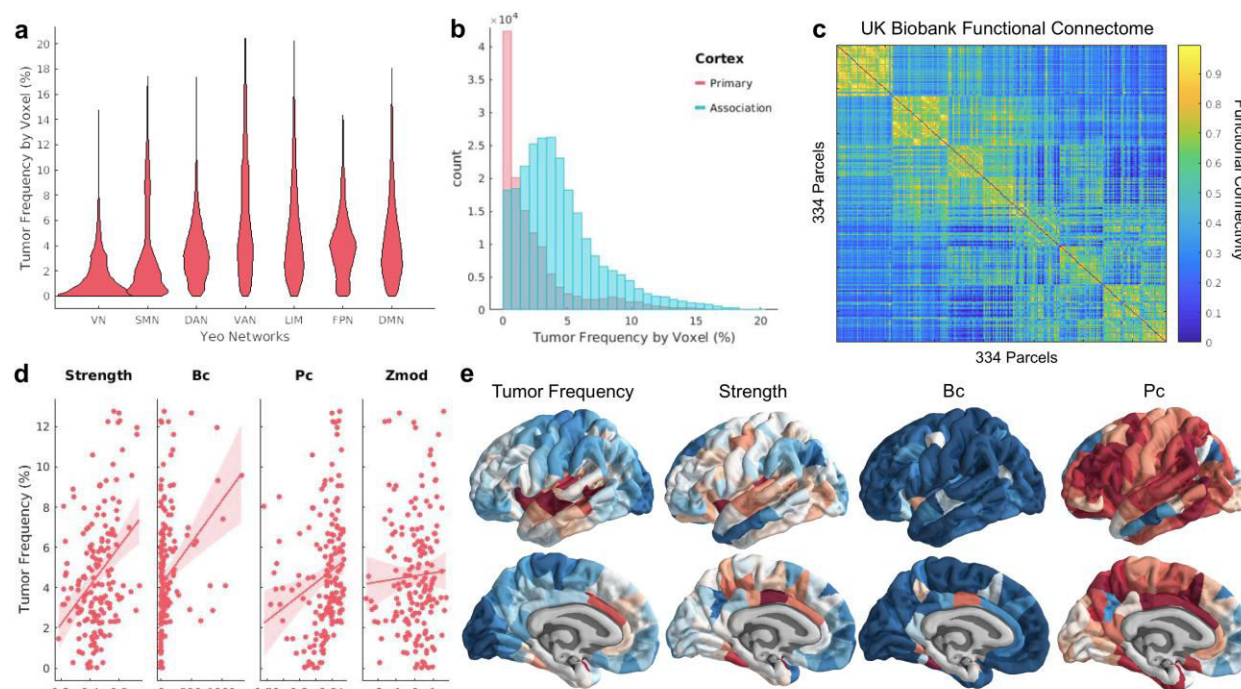


Figure 2. Gliomas localize to connector hubs of the brain. A. Violin plot comparing glioma frequency distributions across canonical subnetworks. B. Histogram comparing glioma frequency distribution across primary versus association cortex. C. Functional connectome calculated from resting state functional scans of over 4000 UK BioBank participants. Nodes in the network are organized according to their affiliation with different canonical subnetworks. D. Correlations between glioma frequency and hub measures calculated from the functional connectome. E. Visualization of glioma frequency and functional hub measures on the cortical surface.

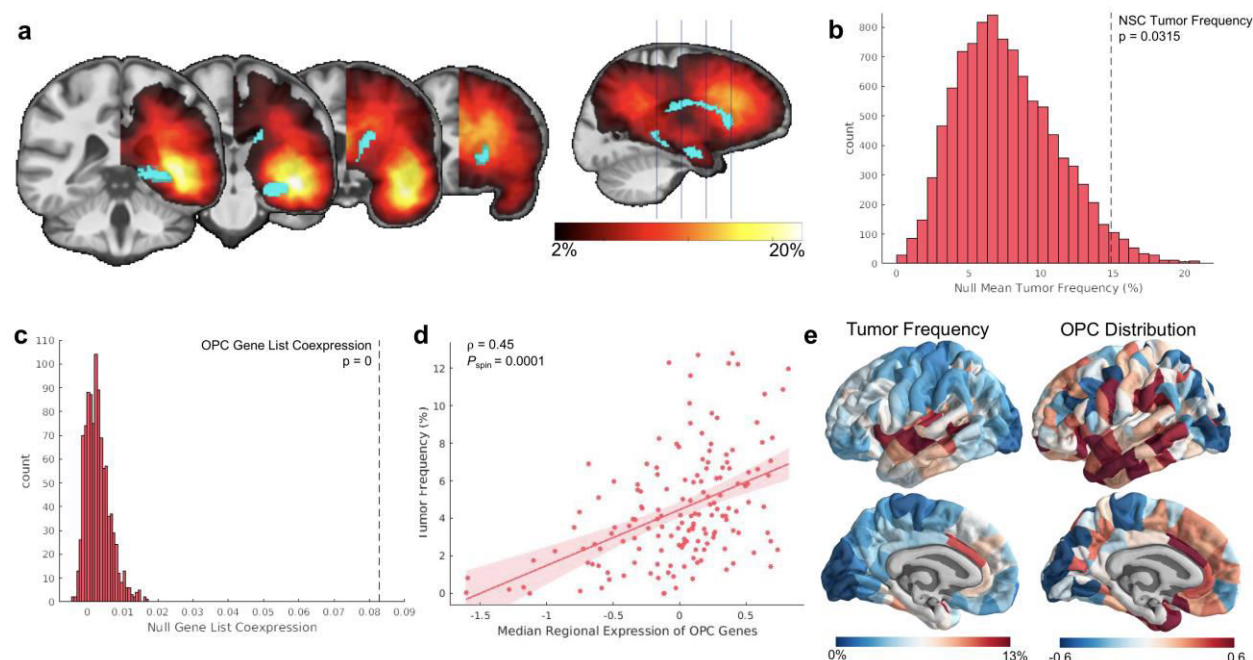


Figure 3. Gliomas localize to brain regions enriched with stem-like cells. A. Visualization of the parcel masks representing the hippocampus and caudate superimposed on the mirrored tumor frequency map. B. Average tumor frequency across the hippocampus and caudate (represented as the dotted black line) compared to a distribution of average tumor frequency across 10000 sets of two randomly chosen parcels. C. Co-expression among genes within the OPC gene list compared to co-expression among 10000 identically-sized sets of genes. D. Correlation between OPC enrichment across cortex and glioma frequency ($\rho = 0.45$; $P_{\text{spin}} = 0.0001$). E. Visualization of glioma frequency and OPC enrichment on the cortical surface.

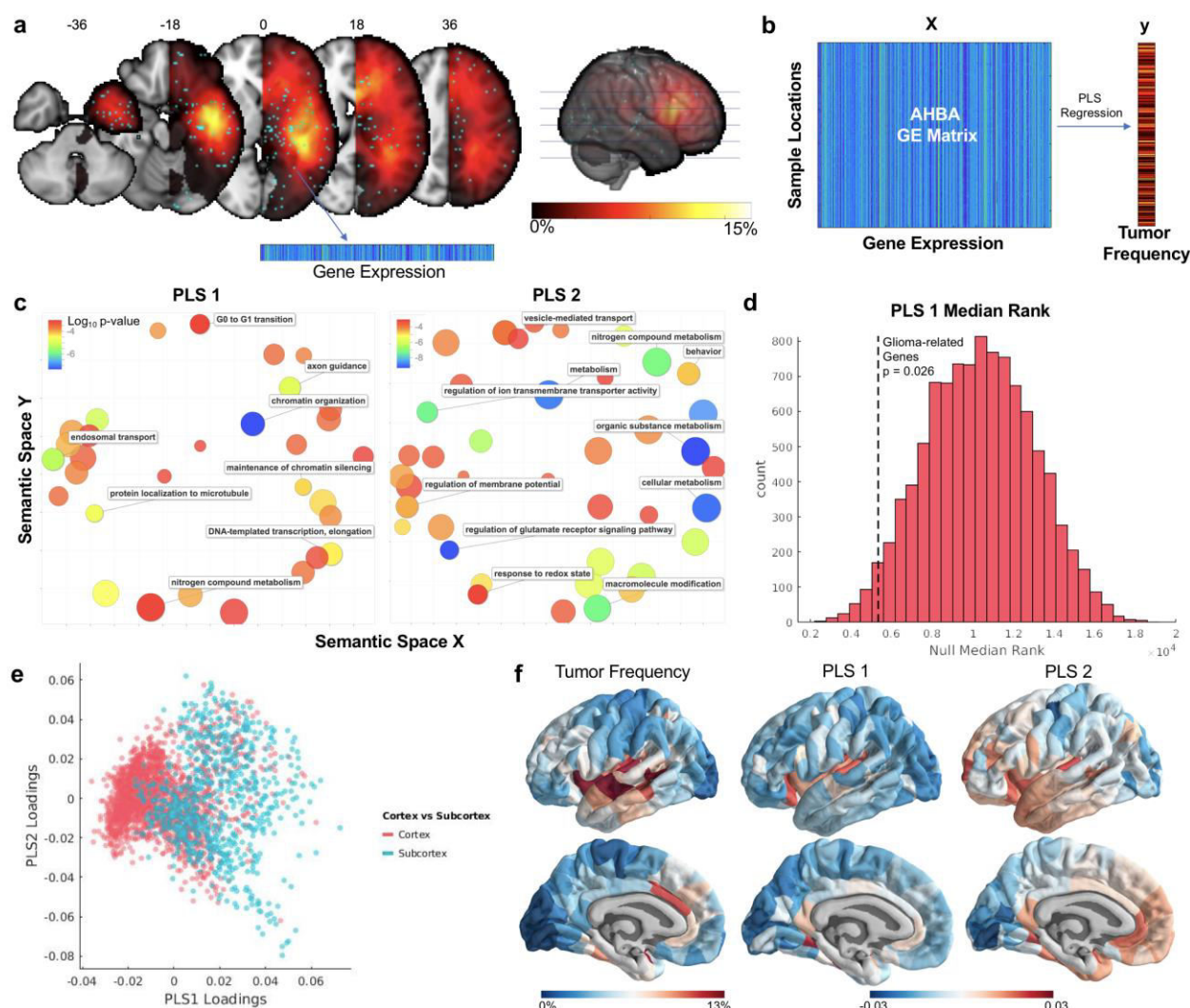


Figure 4. Transcriptomic correlates of glioma frequency. A. Alignment of AHBA sample locations to the tumor frequency map. B. Illustrative flowchart of the statistical analysis to relate normative spatial gene expression patterns to glioma frequency. C. Gene ontology terms associated with two partial least squares components (PLS1 and PLS2) that relate gene expression with glioma frequency. D. Median rank of 13 genes commonly altered in glioma compared to null distribution of median ranks. D. AHBA samples plotted by PLS1 loadings, PLS2 loadings, and cortex versus subcortex. Samples were assigned as cortex or subcortex depending on their overlap with extensively smoothed masks of these regions. E. Visualization of glioma frequency, PLS1 loadings, and PLS2 loadings on the cortical surface. F. PLS loadings from samples were interpolated to parcels via a nearest neighbor mapping.